

**A THEORETICAL STUDY OF ANOMALOUS NERNST
CONDUCTIVITY WITH A WEYL-SEMIMETAL PHASE IN
Co₂YSb HEUSLER ALLOY**

**A DISSERTATION
SUBMITTED IN PARTIAL FULFILLMENT OF THE REQUIREMENTS FOR
THE AWARD OF THE DEGREE
OF
MASTER OF SCIENCE
IN
PHYSICS**

Submitted by:

**GAURAV KUMAR
2K23/MSCPHY/22**

**Under the supervision of
Dr. MUKHTIYAR SINGH**
Assistant Professor



DEPARTMENT OF APPLIED PHYSICS

**DELHI TECHNOLOGICAL UNIVERSITY
(Formerly Delhi College of Engineering)
Bawana Road, Delhi-110042**

JUNE, 2025

DELHI TECHNOLOGICAL UNIVERSITY

(Formerly Delhi College of Engineering)

Bawana Road, Delhi-110042

CANDIDATE'S DECLARATION

I GAURAV KUMAR, Roll No. 2K23/MSCPHY/22 student of M.Sc. (Physics), hereby declare that the project Dissertation titled “A theoretical study of Anomalous Nernst Conductivity with a Weyl-Semimetal Phase in Co_2YSb Heusler alloy” which is submitted by me to the Department of Applied Physics, Delhi Technological University, Delhi in partial fulfilment of the requirement for the award of the degree of Master's in Physics is original and not copied from any source without proper citation. This work has not previously formed the basis for awarding any Degree, Diploma Associateship, Fellowship, or other similar title or recognition.

The work has been accepted in a peer-reviewed Scopus-indexed conference with the following details:

Title of Paper: “A theoretical study of Anomalous Nernst Conductivity with a Weyl-Semimetal Phase in Co_2YSb Heusler alloy”

Authors' names (in sequence as per research paper): Gaurav Kumar, Kulwinder Kumar, and Mukhtiyar Singh.

Name of conference / Journal: 3rd International Conference on Advanced Functional Material and Devices for sustainable development (AFMD-2025)

Have you registered for conference (Yes/No): Yes

Status of paper (Accepted/Published/comment): Accepted

Date of communication: April 24, 2025

Date of acceptance: June 8, 2025

Date of publication: Yet to be published

Place: Delhi

GAURAV KUMAR

Date: 09/06/2025

(2K23/MSCPHY/22)

This is to certify that the student has incorporated all the corrections suggested by the examiners in the thesis and that the statement made by the candidate is correct to the best of our knowledge.

DR. MUKHTIYAR SINGH
Supervisor
(Assistant Professor)

ACKNOWLEDGEMENT

I would like to express my deepest sincere gratitude to my supervisor, Dr. Mukhtiyar Singh, Assistant Professor, Department of Applied Physics, Delhi Technological University for allowing me to work under his guidance and for constant inspiration and incessant support throughout the project. I take this opportunity to express our indebtedness to my supervisor for his enthusiastic help, expertise, brilliant ideas, valuable suggestions, and constant encouragement. I am grateful to acknowledge the constant help and convenience at every step of our project by all the lab members (PhD scholars), Dept. of Applied Physics. Lately, I am thankful to our families and friends for their love, care, and support who patiently extended all sorts of help for accomplishing this task.

GAURAV KUMAR
(2K23/MSCPHY/22)

ABSTRACT

Magnetic Weyl semimetals (WSM) are a distinctive category of topological quantum materials that exhibit pairs of non-degenerate band-crossing points, called as Weyl nodes. A defining feature of WSM is the presence of symmetry-protected Fermi arcs that connect Weyl nodes of opposite chirality. We conduct a systematic investigation of the electronic, magnetic, Topological, and anomalous transport properties of Co_2YSb Full Heusler alloy through the Density Functional Theory. The spin-polarised density of states reveals the half-metallicity and ferromagnetic nature of the material. The electronic structure indicates the presence of Topological Nodal lines, which are gapped out with the inclusion of Spin-Orbital coupling (SOC). To probe the Topological characteristics of Co_2YSb , we conduct a Wannier-function-based tight-binding calculation with the effect of SOC and obtain the 12 pairs of Weyl nodes of opposite chirality. The presence of symmetry protected Topological Fermi arc and surface state confirms the Weyl semi-metallic nature of this material. Furthermore, the anomalous Hall and Anomalous Nernst conductivity are computed along the (001) plane. Therefore, our work highlights the interplay between topology and anomalous transport phenomena in the systematic investigation of the electronic, magnetic, Topological, and anomalous transport properties of Co_2YSb magnetic Heusler alloys, with their wide applications in spintronics and thermoelectric devices.

Keyword: - Weyl semimetal, Weyl nodes, Anomalous Hall effect, Anomalous Nernst effect, Berry curvature.

CONTENTS

Title	Page No.
Candidate Declaration and Supervisor Certificate	ii
Acknowledgment	iii
Abstract	iv
Table of Contents	v
List of Figures	vii
List of Tables	viii
List of Symbol and Abbreviations	ix

CHAPTER 1.....1-7

INTRODUCTION AND OBJECTIVES

1.1. INTRODUCTION

1.2. LITERATURE REVIEW

1.2.1. Weyl semimetal

1.2.2. Advantages

1.2.3. Disadvantages

CHAPTER 2..... 8-10

MATERIALS AND CALCULATION

2.1. Materials

2.2. Calculation

CHAPTER 3..... 11-18

RESULTS AND DISCUSION

3.1. Structural Properties

3.2. Electronic, Magnetic and Topological Properties

3.3. Berry Curvature, Anomalous Hall and Nernst conductivity

CHAPTER 4.....19-20

CONCLUSION

4.1. Conclusion

4.2. Future scope

REFERENCES.....21-24

APPENDIX.....25-30

LIST OF FIGURES

Figure 1 (a) displays the lattice parameter optimization curve, showing the dependence of energy as a function of lattice parameter for both the Xa and $L2_1$ structural phases. (b) The electronic density of states (DOS) for $L2_1$ structure Co_2YSb Heusler alloy.....21

Figure 2 (a) displays the electronic band structure calculated using GGA+U without SOC, where the black and red lines correspond to the up-spin and down-spin channels, respectively. In panel (b), the corresponding SOC-included band structure is presented. An enlarged view highlighted circle area for both band structures displays in the blue box.....23

Figure 3 (a) displays the Fermi surface spectral function along the high-symmetry path $X-\Gamma-X$, while panel (b) presents the corresponding Fermi surface contour at the Fermi level ($E_F = 0.0$ eV), calculated with spin-orbit coupling.....24

Figure 4 (a) The energy-momentum relationships in proximity to the Fermi surface (upper panel) using spin-orbit-interacting electron dispersion relations alongside the k -resolved Berry flux density (Ω_z) mapped along principal symmetry axes (lower panel), (b) The variation of the intrinsic anomalous Hall conductivity (σ_{xy}^A) with the chemical potential ($E-E_F$) in full Brillouin zone integration within a ± 0.50 eV energy window centred at the Fermi energy. (c) The dependence of the anomalous Nernst conductivity (α_{xy}^z), with the chemical potential ($E-E_F$) within a ± 0.50 eV energy window at different temperatures and (d) The variation of α_{xy}^z as a function of temperature at E_F 27

LIST OF TABLES

Table 1. This table summarizes the 12 pairs of Weyl points, providing their precise momentum-space (k-space) coordinates along with the corresponding topological chirality.....	25
---	----

LIST OF SYMBOLS AND ABBREVIATIONS

TSM	Topological semimetal
E_F	Fermi level
IS	Inversion symmetry
TRS	Time reversal symmetry
AHE	Anomalous Hall Effect
ANE	Anomalous Nernst Effect
AHC	Anomalous Hall Conductivity
ANC	Anomalous Nernst Conductivity
NLWS	Nodal line Weyl semimetal
SOC	Spin orbit coupling
VASP	Vienna ab initio simulation package
DFT	Density Functional Theory

CHAPTER 1

INTRODUCTION AND OBJECTIVES

1.1. INTRODUCTION

In the field of condensed matter physics, the topological semimetals (*TSM*) have gained considerable attention owing to their promising applications in quantum computing, low-dissipation electronics, spintronics, and energy harvesting systems [1-2]. Like the topological insulator, TSM also exhibits exotic features like band inversion, Symmetry-protected Fermi arc, topological surface states, etc. [3]. Furthermore, TSMs are categorized into different categories based on the dimension of topological surface state: a nodal point is a zero-dimensional, a Nodal line with one dimension, and a nodal surface with two dimensions [4-6]. For instance, they can also be divided as Dirac, Weyl, triply, and higher-fold states based on the topological state band degeneracy [7-8]. In these systems, the conduction and valence bands intersect linearly at discrete points called Dirac or Weyl nodes, or along high-symmetry lines within the Brillouin zone, maintaining their gapless characteristics in proximity to the Fermi level (E_F). Importantly, Dirac points divide into pairs of Weyl nodes of opposite chirality, which refers as a Weyl semimetal (WSM), when either inversion symmetry (IS), time-reversal symmetry (TRS), or both are broken [9-13]. The hallmark of these WSMs is the emergence of the Fermi arc, a surface states that form open trajectories connecting the projected positions of two Weyl nodes of opposite chirality. The Weyl nodes always appear in pairs with opposite chirality and act as sources and sinks of Berry curvature. This Berry curvature also serves as the intrinsic mechanism of a

variety of exotic electrical and thermal transport phenomena, like anomalous Hall effect (*AHE*) and anomalous Nernst effect (*ANE*), respectively. The *AHE* manifests as a transverse voltage that is perpendicular to an applied current without any external magnetic field, distinguishing it from the conventional Hall effect, which is driven by the Lorentz force [14-15]. In a similar manner, the *ANE* generates a transverse voltage in response to a temperature gradient, rather than an electric current [16]. Shi *et al.* demonstrated that *Ti₂MnAl* exhibits a substantial Berry curvature, leading to a significant anomalous Hall conductivity (*AHC*) [17]. More recently, in 2023, Shukla *et al.* reported an exceptionally large *AHC* and Anomalous Nernst Conductivity (*ANC*) in *Cu₂CoSn*, both theoretically and experimentally [18]. Additionally, the Heusler alloy *Co₂MnGa* has exhibited a remarkable *AHC* and the highest recorded *ANC* to date, as validated by experimental investigations employing angle-resolved photoemission spectroscopy [19-21]. Heusler alloys are an intermetallic system that possesses net non-zero magnetic moments without hosting any magnetic entity; in addition, they also show features high magnetic saturation, high spin polarization, high Curie temperature, and high thermoelectric coefficients [22-24]. Magnetic materials naturally exhibit the breaking of *TRS*, due to the presence of ferromagnetic ordering, which may exhibit the *WSM* and nodal line semimetal (*NLSM*) types of topological phases. In the literature, many other studies have been presented on *WSM*, which linked the origin of *AHC* and *ANC* with the topological aspect of the materials[25-28]. Structurally, these Heusler materials fall into two primary categories: (1) half-Heusler compounds (*XYZ*) with a *1:1:1* stoichiometry that adopt a non-centrosymmetric cubic structure, and (2) full-Heusler compounds (*X₂YZ*) with a *2:1:1* composition. Generally, full-Heusler alloys exhibit two types of cubic structural phases, *L2₁* and *Xa*, which are

characterized by four interpenetrating face-centred cubic sublattices. In $L2_1$ arrangement, two X atoms are positioned at the $(1/4, 1/4, 1/4)$ and $(3/4, 3/4, 3/4)$, while the Y and Z atoms are located at the $(1/2, 1/2, 1/2)$ and $(0, 0, 0)$ Wyckoff sites, respectively. Conversely, in the case Xa -type structural phase, two X atoms are positioned at $(0, 0, 0)$ and $(1/4, 1/4, 1/4)$, with the Y and Z atoms located at $(1/2, 1/2, 1/2)$ and $(3/4, 3/4, 3/4)$ Wyckoff sites. The electronic structure of full-Heusler alloys is associated with distinctive topological properties, characterized by significant AHC that arise from substantial Berry curvature in proximity to the E_F . This behaviour is a consequence of their spin-polarized band structure and strong spin-orbit coupling (SOC), rendering them particularly valuable for the exploration of topological magnetism and the advancement of electronic devices. The Full Heusler compounds Co_2MnGa , Co_2MnAl , Co_2TiGe , and Co_2TiSi have been demonstrated, both theoretically and experimentally, to exhibit Weyl semimetal characteristics, which further contribute to elevated values of AHC and ANC [29-32]. Within the family of Co_2 -based half-metallic ferromagnets, Co_2YSb has emerged as a particularly intriguing material due to its distinctive structural and magnetic properties [33]. Notably, before this investigation, no comprehensive study had been reported on the topological nature and its associated anomalous Hall and Nernst effects in this system. Motivating, by this we present a systematic investigation of Weyl characteristic and the AHC and ANC in Co_2YSb Heusler alloy. Our investigation reveals the remarkable presence of topological features like Weyl nodes and topological symmetry protected surface states. Further, we also calculate the AHC and ANC arising from the strong Berry curvature originate from the Weyl nodes along (001) plane. Therefore, our findings

suggest that Co_2YSb is a *WSM* and a potential candidate for thermoelectric and spintronic applications.

1.2. LITERATURE REVIEW

The Anomalous Hall Effect represents a fascinating quantum transport phenomenon where electric current flowing through a magnetic material generates a perpendicular voltage without requiring an external magnetic field, unlike the conventional Hall effect. This effect emerges from the complex interplay between magnetism, spin-orbit coupling, and the scattering mechanisms within the material, fundamentally stemming from the asymmetric deflection of electrons based on their spin orientations. The theoretical foundation was established through the pioneering work of Karplus and Luttinger in the 1950s, who identified both intrinsic contributions independent of scattering and extrinsic mechanisms involving asymmetric impurity scattering. The effect originates from magnetic interactions between localized d-electrons and conduction electrons, involving magneto-static interactions, sp-d exchange interactions, and crucially, spin-orbit coupling.

The Anomalous Nernst Effect serves as the thermoelectric counterpart to the anomalous Hall effect, manifesting when a temperature gradient applied across a magnetic material generates an electric voltage perpendicular to both the heat flow direction and the magnetization vector. This phenomenon was traditionally understood to be proportional to the material's magnetization, but recent theoretical advances have revealed that it more fundamentally originates from the Berry curvature of electronic bands near the Fermi level. The effect has demonstrated remarkable potential in

topological materials, with compounds like Co_2MnGa achieving anomalous Nernst thermopower values of approximately $6.0 \mu\text{V K}^{-1}$ at room temperature, representing a seven-fold enhancement over conventional ferromagnets. This enhancement occurs due to the large net Berry curvature associated with nodal lines and Weyl points in the electronic structure, transcending the traditional magnetization-scaling relationship.

Weyl semimetals constitute a revolutionary class of topological materials where valence and conduction bands intersect at discrete points called Weyl nodes, creating quasiparticle excitations that behave as Weyl fermions. These materials exhibit linear energy-momentum dispersion relations, making electrons behave like massless relativistic particles even at room temperature. The Weyl fermions possess distinct chirality that act as topological charges, creating monopoles and anti-monopoles of Berry curvature in momentum space. A defining characteristic of Weyl semimetals is the presence of topological surface states known as Fermi arcs, which are discontinuous segments of the two-dimensional Fermi contour terminated at the surface projections of Weyl nodes. The first experimental observation was achieved in tantalum arsenide (TaAs) in 2015, establishing the existence of both Weyl fermions and Fermi arc surface states through direct electronic imaging. These materials have since expanded to include various compounds such as Co_2TiGe , MoTe_2 , WTe_2 , and several others, each offering unique electronic properties and potential applications in next-generation quantum devices.

1.2.2. Advantages

- **Field-Controllable Electronic Properties:**

These materials offer the unique capability of modulating their electronic behaviour through applied electric fields, opening pathways for advanced spintronic devices and memory storage technologies that can be electrically switched.

- **Outstanding Charge Transport Characteristics:**

Weyl semimetals demonstrate remarkable electrical properties including extremely high carrier velocities and minimal scattering resistance, as charge carriers behave like massless relativistic particles moving at extraordinary speeds.

- **Unique Quantum Transport Effects:**

These systems host distinctive quantum phenomena such as chiral magnetic responses, unconventional magnetoresistance behaviour, topological Hall states, and novel oscillatory patterns in electrical transport measurements.

- **Enhanced Hall Response in Weak Magnets:**

Certain compounds like $\text{Co}_3\text{Sn}_2\text{S}_2$ demonstrate unusually strong anomalous Hall responses reaching hundreds of $\Omega^{-1}\text{cm}^{-1}$ despite possessing only modest magnetic moments, attributed to their multiple Weyl node configurations.

- **Controllable Magnetic State Transitions:**

non-collinear antiferromagnetic systems allow manipulation of different magnetic configurations through chemical doping, mechanical strain, or spin-polarized currents, each exhibiting distinct Hall conductivity signatures.

1.2.3. Disadvantage

- **AI Ambiguous Topological Character:**

Real materials often exhibit Fermi surfaces that connect multiple Weyl points, making the fundamental chiral properties undefined and complicating the identification of genuine topological transport signatures.

- **Sample Quality Dependencies:**

Material imperfections and compositional variations can generate misleading Hall measurement artifacts that mimic topological effects, creating challenges in distinguishing authentic phenomena from experimental noise.

- **Field-Induced Current Redistribution:**

Strong magnetic fields can cause non-uniform current flow patterns that deflect electrical current along field directions, introducing systematic errors in magneto transport characterization.

- **Multi-Band Transport Complexity:**

The coexistence of electron and hole carriers from overlapping valence and conduction bands necessitates sophisticated analytical approaches, as conventional single-carrier Hall analysis becomes inadequate.

- **Intrinsic Conductivity Constraints:**

The short electron mean free paths characteristic of frustrated magnetic systems impose fundamental limits on achievable Hall conductivities, typically capping values at approximately one conductance quantum per atomic layer.

CHAPTER - 2

MATERIALS AND METHODS

2.1. Materials

Co₂YSb stands as a remarkable representative within the full Heusler alloy category, extensively analysed through sophisticated first-principles density functional theory methodologies. The groundbreaking research conducted by D. P. Rai and R. K. Thapa, featured in the Chinese Journal of Physics, provided comprehensive insights into the half-metallic ferromagnetic characteristics of this compound using state-of-the-art computational techniques. The material adopts the distinctive L21-type cubic crystallographic arrangement, a hallmark of full Heusler compounds following the X₂YZ stoichiometric formula, which facilitates optimal magnetic alignment and electronic band organization essential for achieving half-metallic properties.

Within the broader context of Co₂-based Heusler materials, Co₂YSb has garnered significant attention as a leading candidate for advanced spintronic technologies owing to its exceptional electronic characteristics. The theoretical investigations utilized the full-potential linearized augmented plane wave computational method incorporated within the LSDA+U theoretical framework to achieve precise ground state property predictions. This sophisticated approach was deliberately selected after conventional LSDA and GGA methodologies demonstrated limitations in accurately characterizing the strongly correlated d-electron systems inherent in these magnetic materials, making the enhanced computational strategy indispensable for reliable half-metallic behaviour forecasting.

1.2. Computational Details

The first-principles calculations were performed to investigate the electronic, magnetic, Topological and transport properties of Co_2YSb Heusler alloy. Density functional theory (*DFT*) is used which is implemented in the Vienna ab initio simulation package (*VASP*), employing the projector augmented-wave (*PAW*) method [34-36]. Further, the exchange-correlation effects were treated within the generalized gradient approximation (*GGA+U*) using the Perdew-Burke-Ernzerhof (*PBE*) functional, where calculated Hubbard U and exchange J parameters were approximately 3.94 and 0.81 eV for cobalt (*Co*), and 0.04 and 0.81 eV for yttrium (*Y*), respectively [37]. In order to perform spin-polarized calculations and structural optimization, a convergence criterion for the self-consistent field energy of 10^{-5} eV was set. For the plane wave basis, the energy cut-off value was set to 520 eV. A fully optimized Γ -centred k-mesh grid of $11 \times 11 \times 11$ was used. For a full relativistic approach, we also include the effect of spin-orbital coupling and consider magnetisation along (001) plane. Further, using maximally localized Wannier functions (*MLWFs*), we constructed a tight-binding Hamiltonian by Wannier90 code. The WannierTools package was used to calculate the transport properties and identify the Weyl nodes within the bulk electronic structure, as well as the surface Fermi arc, thereby confirming the topological nature of the system [38]. In addition, the Berry curvature distributions are calculated using the Kubo formulation as given below [39]:

$$\Omega_{ij}^n(k) = \sum_{n \neq m} \frac{\langle n | \frac{\partial H}{\partial k_i} | m \rangle \langle m | \frac{\partial H}{\partial k_j} | n \rangle - (i \leftrightarrow j)}{(E_n - E_m)^2} \quad (1)$$

where $|n\rangle$ and $|m\rangle$ are the eigenstates of the Hamiltonian H , while E_n and E_m denote the corresponding energy eigenvalues. The AHC and ANC were evaluated using WannierTools with a dense $200 \times 200 \times 200$ k -mesh for high precision using the given equations 2 and 3, respectively [40,14].

$$\sigma_{xy}^A = \frac{-e^2}{\hbar} \int_{BZ} \frac{d^3k}{(2\pi)^3} f(k) \Omega_B(k) \quad (2)$$

$$\alpha_{xy}^A = -\frac{1}{e} \int_{BZ} d\varepsilon \frac{\partial f(\varepsilon-\mu, T)}{\partial \varepsilon} \frac{\varepsilon-\mu}{T} \sigma_{xy}^A(\varepsilon) \quad (3)$$

Where f is the Fermi-Dirac distribution function, μ is the chemical potential, \hbar is the reduced Planck constant, e is the electron charge, and the integration is performed over the entire Brillouin zone. The temperature T and chemical potential μ govern the statistical distribution of electrons in the system.

CHAPTER - 3

CALCULATION AND RESULTS

3.1. Results and Discussion

3.1.1. Structural Properties

Firstly, we perform the structural optimization calculation to identify the stable structural phase and equilibrium lattice parameter for Co_2YSb Heusler alloy. Fig. 1 (a) illustrates the variation of thermodynamic free energy concerning the lattice parameter

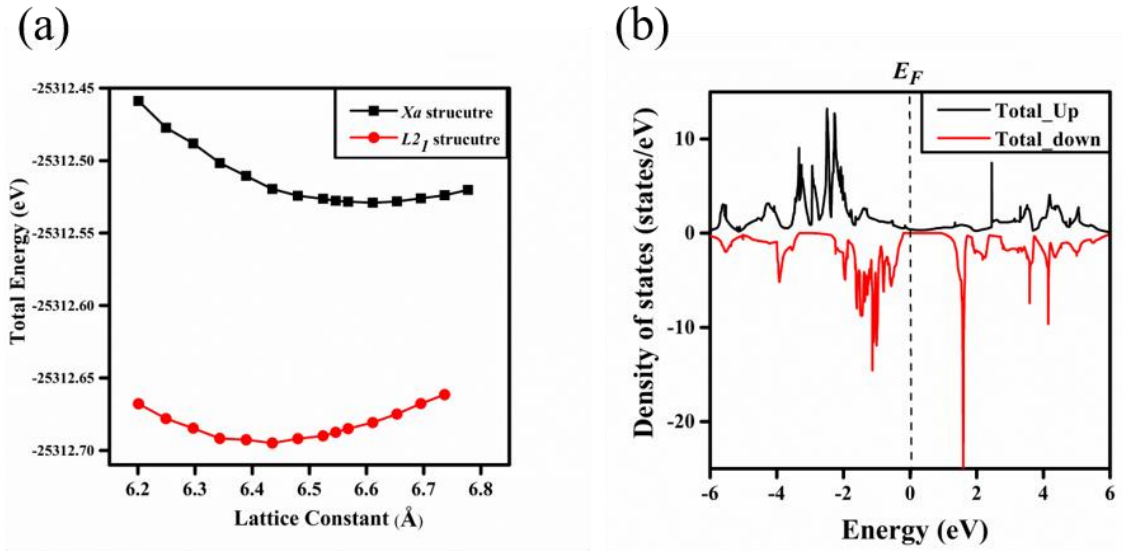


Figure 1 (a) displays the lattice parameter optimization curve, showing the dependence of energy as a function of lattice parameter for both the Xa and $L2_1$ structural phases. (b) The electronic density of states (DOS) for $L2_1$ structure Co_2YSb Heusler alloy.

for both structural phases $L2_1$ and Xa . The energy vs lattice parameter curve suggests that the $L2_1$ structure is relatively more stable than the Xa structure due to the more

negative value of energy of the $L2_1$ structure. The minima of the curve represent the corresponding equilibrium lattice parameter values 6.43 \AA and 6.61 \AA for $L2_1$ and Xa structural phases, respectively. These obtained values of lattice constant are in close agreement with the previously reported theoretical work for this material [33]. And we perform the rest of the calculations for $L2_1$ structural, which is the most stable structural phase of Co_2YSb Heusler alloy.

3.1.2. Electronic, Magnetic, and Topological properties

Now, to investigate the electronic and magnetic properties, we perform the spin polarization calculation for Co_2YSb . The Density of state (DOS) is plotted in Fig. 1 (b), with majority-spin (\uparrow) channel represented by black and minority-spin (\downarrow) channels in red colour line. DOS reveals that the Co_2YSb alloy exhibits a half-metallic characteristic in which the majority spin channel is conducting, and the minority spin channel exhibits a semiconducting band of value 1.47 eV . This half-metallic behaviour is also confirmed from Fig. 2 (a), in which spin spin-polarized electronic band structure is plotted against high-symmetry k -path.

Furthermore, the total magnetic moments (M_t) consistently exhibit the values of $2 \mu_B$, which is in excellent agreement with the Slater-Pauling rule as given below [42-43]:

$$M_t = Z_t - 24 \quad (4)$$

where Z_i represents the total valence electrons (26) from constituent atoms ($Co:9$, $Y:3$, $Sb:5$). The primary contribution to M_i originates from Co atoms, driven by significant exchange splitting between majority and minority spin states, while the Sb anion provides minor contributions. Notably, the Y element displays a negative local magnetic moment, indicating antiparallel alignment relative to Co and Sb moments. This ferrimagnetic coupling between transition metals arises from opposing interactions during exchange splitting, as evidenced by the contrasting signs of Co and Y magnetic moments. The interstitial regions exhibit negligible magnetic moments, confirming the localized character of the magnetic behaviour.

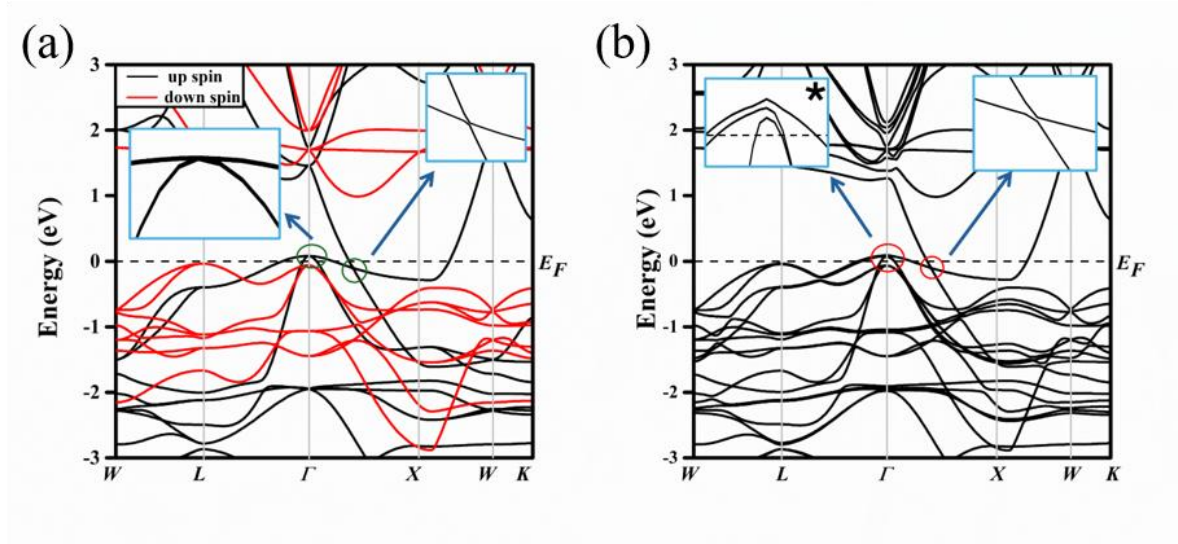


Figure 2 (a) displays the electronic band structure calculated using GGA+U without SOC, where the black and red lines correspond to the up-spin and down-spin channels, respectively. In panel (b), the corresponding SOC-included band structure is presented. An enlarged view highlighted circle area for both band structures displays in the blue box

Further, to explore the topological feature in Co_2YSb Heusler alloy, we also include the effect of SOC in the calculations. Many linear bands are crossing from the nodal lines present in the electronic band structure in the absence of SOC . Near the E_F the

non-trivial linear band crossing are marked by green circle without *SOC* effect as shown Fig. 2 (a) and inset shows the enlarge view of non-trivial linear band crossings. Now, we consider the *SOC* and magnetisation along (001) plane therefore, *SOC* lifting the degeneracy along $K_x = 0$ and $K_y = 0$ plane, hence, the nodal line remains gapless along $K_z = 0$ plane [44]. Fig. 2 (b), displays the electronic band structure along high-symmetry k -path, with the presence of *SOC*. The linear band dispersions are gapped out along L to Γ and Γ to X path, marked by the red circle as shown in Fig. 2

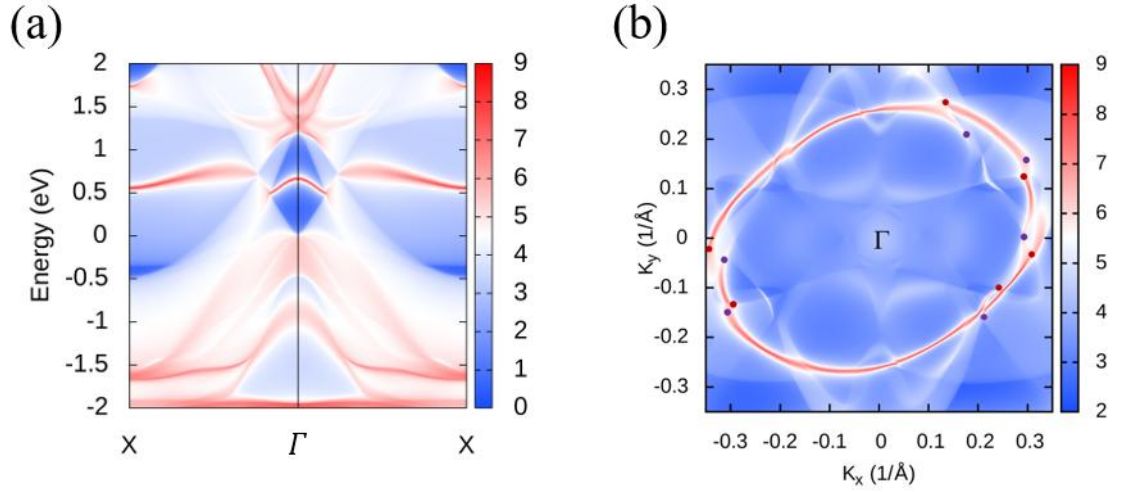


Figure 3 (a) displays the Fermi surface spectral function along the high-symmetry path $X-\Gamma-X$, while panel (b) presents the corresponding Fermi surface contour at the Fermi level ($E_F = 0.0$ eV), calculated with spin-orbit coupling.

(b), and inset shows the enlarged view of the band dispersion. In the space group 225, the point group crystal symmetry of Co_2YSb contained three C_4 rotation axes and three mirror planes along $M_x(K_x = 0)$, $M_y(K_y = 0)$ and $M_z(K_z = 0)$ in the absence of *SOC*. These mirror planes provide the symmetry protection to the gapless nodal lines in the band dispersion in $K_x = 0$, $K_y = 0$ and $K_z = 0$ planes. Now with the effect of *SOC* along (001) plane, the crystal system only preserves the mirror symmetry $M_z = 0$ and C_4^Z rotational symmetry. Therefore, along the $K_x = 0$, $K_y = 0$ planes, minimum

two nodal lines are expected to be gapped out, and along the $K_z = 0$ plane, the nodal line should be preserved. However, *SOC* induced a smaller gap in the nodal line as shown in Fig. 2 (b). Using the MLWF, we obtained the projected Fermi surface of the (100) surface, in which one can observe a gapped, distorted nodal line with 6 Fermi arcs connecting the $12; W(+1)$ and $W(-1)$ nodes, as shown in Fig. 3 (b). In addition, we obtain the total 12 pairs of Weyl nodes with opposite chirality $+1$ and -1 as listed in Table 1 with locations in energy and momentum coordinates. Further, we also calculate the projected surface spectrum on the (100) surface of Co_2YSb along L to Γ and Γ to X path which is shown in Fig. 3 (a). We observe a topological surface state, which connects two Weyl nodes of opposite chirality around the Γ point. Therefore, the presence of Weyl nodes and nodal lines in Co_2YSb Heusler alloys characterizes this material as a newly predicted *WSM* candidate.

Table 1: This table summarizes the 12 pairs of Weyl points, providing their precise momentum-space (k-space) coordinates along with the corresponding topological chirality.

S.N.	K_x	K_y	K_z	Chirality	K_x	K_y	K_z	Chirality
1	-0.23357	-0.16271	0.23619	-1	-0.24425	-0.10191	0.23499	1
2	0.32648	-0.01899	0.02656	-1	0.32826	0.00507	-0.01144	1
3	-0.24814	0.19649	-0.16581	-1	0.25414	0.13005	-0.21859	1
4	-0.01363	0.28774	0.20529	-1	0.0384	-0.26269	-0.23435	1
5	0.23097	-0.05481	0.23952	-1	-0.21862	-0.21725	0.11444	1
6	-0.16362	-0.10265	-0.27289	-1	-0.16324	0.10197	0.27275	1
7	-0.20616	-0.00831	0.25222	-1	-0.10717	0.30238	0.08536	1
8	0.01464	-0.29473	-0.19412	-1	-0.05756	0.19091	-0.27373	1
9	0.07826	0.18495	-0.26322	-1	-0.04876	-0.18776	0.2674	1
10	0.22842	-0.22384	0.12193	-1	0.15743	-0.29586	-0.01605	1
11	0.17034	-0.09026	-0.27355	-1	0.13808	0.13757	0.26624	1
12	0.28918	0.11521	-0.16529	-1	0.28559	-0.11717	0.17809	1

3.1.3. Berry Curvature, Anomalous Hall and Anomalous Nernst Effect:

Now, the *AHE* is a consequence of intrinsic mechanisms in which *AHC* is proportional to Berry curvature, a geometrical feature of energy bands. Fig. 4 (a) displays the berry curvature plot along the high-symmetry k -path calculated from equation 1. Generally, Berry curvatures originate from the pair of bands in which one is occupied, and another is unoccupied at the E_F . The magnitude of the Berry curvature peak depends on the energy gap induced by the *SOC* effect. Similarly, in the case with the Nodal line, which gapped out into a pair of Weyl points, and which is the source of Berry curvature. The Berry curvature plot contained two major peak, 'A' and 'B' around the high symmetric point Γ . From Fig. 2 (b) (Inset marked by *), there are mainly three bands at E_F , in which peak 'A' with larger magnitude is the consequence of same band gapped out by *SOC* crossing the E_F , in the left side of Γ . However, smaller peak 'B' originates from the two other bands crossing the E_F , in the left side of Γ , which are split by *SOC*, and originally both bands are different as shown in Fig 2(a) in inset without *SOC*. Now, in case *Co₂YSb*, some Weyl nodes lie just below the E_F , and the plot considers the resultant Berry curvature for bands lying at the Fermi level.

Now the *AHC* is calculated using equation 2, Fig. 4 (b) shows the variation of *AHC* with respect to the chemical potential ($E-E_F$) within the energy range of ± 500 meV. At the E_F we obtained the *AHC* value 114.83 S/cm, and one can achieve the maximum value about -586 S/cm just below the E_F at 480 meV. Therefore, this negative of *AHC* value suggests that the overall positive Berry curvature shows the dominance behaviour. In the same manner from equation 3 we have calculated *ANC* for different temperature with respect to the chemical potential ($E-E_F$) within the energy range of

$\pm 500 \text{ meV}$ and plotted in Fig. 4 (c). At room temperature, the value of ANC is 0.34 A/mK at the E_F and obtained maximum value is -2.61 A/mK at just below the E_F about 420 meV . This maximum value of ANC is about 8 times greater than at E_F , which suggest that a slightly modification in the energy level leads large variation in the ANC

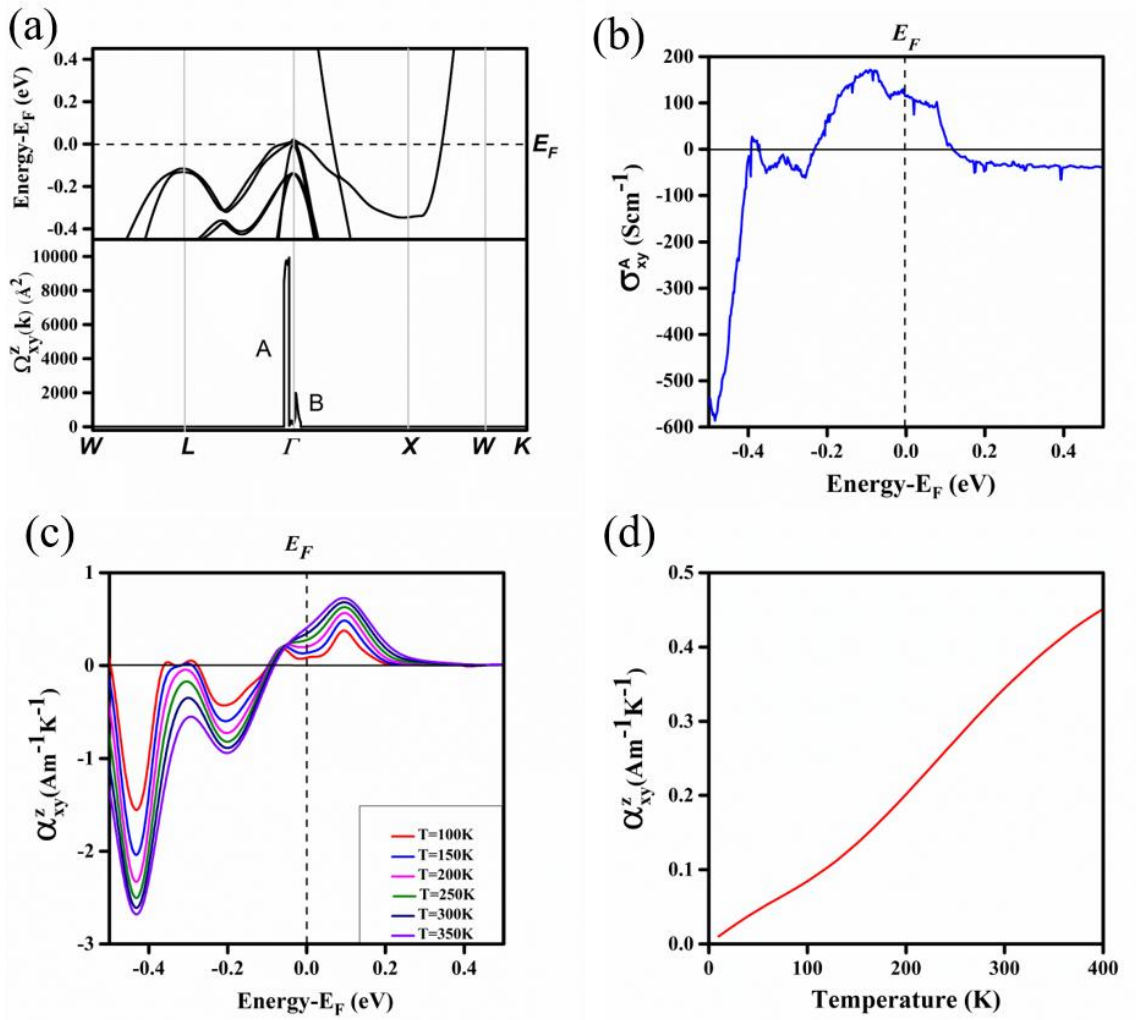


Figure 4 (a) The energy-momentum relationships in proximity to the Fermi surface (upper panel) using spin-orbit-interacting electron dispersion relations alongside the k -resolved Berry flux density (Ω_z) mapped along principal symmetry axes (lower panel), (b) The variation of the intrinsic anomalous Hall conductivity (σ_{xy}^A) with the chemical potential ($E-E_F$) in full Brillouin zone integration within a $\pm 0.50 \text{ eV}$ energy window centred at the Fermi energy. (c) The dependence of the anomalous Nernst

conductivity (α_{xy}^z), with the chemical potential ($E-E_F$) within a ± 0.50 eV energy window at different temperatures and (d) The variation of α_{xy}^z as a function of temperature at E_F .

as shown in Fig. 4 (c). There are two minima in the *ANC* curve below the E_F , one near the -0.18 eV and another at -0.42 eV, both are corresponded to bands that are split by SOC. In addition, we have also plotted the *ANC* dependence with temperature Fig. 4 (d) show that the *ANC* value are increases with temperature, which is good for the room temperature application. These finding for *AHC* and *ANC* are very closely related to other reported work for full Heusler alloy and magnetic topological *WSM*. Now, the *AHC* and *ANC* values are much sensitive to the position of chemical potential and the peak value *AHC* and *ANC* are expected to be at the energy corresponding to Weyl points position with respect to E_F . Therefore, by suitable doping, one can achieve shifting in the E_F and make possible that the Weyl point have come closer to the E_F , which enhance the overall Berry curvature value. Further these large Berry curvature resultants in the large Anomalous Hall and Nernst conductivity. Therefore, over finding suggest that Co_2YSb is a Magnetic *WSM* material, with the large value of *AHC* and *ANC*, which make Co_2YSb a potential candidate for thermoelectric and spintronic application.

CHAPTER – 4

CONCLUSIONS AND FUTURE SCOPE

4.1. Conclusion

This study, is a comprehensive investigation of the presence of Weyl nodes, as well as the anomalous Hall and Nernst conductivities in the full Heusler alloy Co_2YSb . Our first-principles calculations reveal that the $L2_1$ structural phase is the most stable phase for Co_2YSb , in which it exhibits the half-metallic ferromagnetism characteristics. The spin-polarized band structure shows the presence of nodal lines, which are gapped out with the effect of spin-orbital coupling along the (001) plane. Further, Topological features like Fermi arc and surface state are computed using the maximally localized Wannier functions along the (100) plane. We identify a distorted, broken Fermi arc that connects the number of Weyl pairs of opposite chirality in the Fermi surface. In addition, we also obtained 12 pairs of Weyl nodes having the opposite chirality (± 1) in the bulk Brillouin zone, which confirms the Weyl semi-metallic nature of Co_2YSb Heusler alloy. The calculated Berry curvature, derived from the Kubo formalism, underpins the emergence of notable transport phenomena, including the AHC and ANC . At the E_F , the AHC exhibits a value of 114.83 S/cm , while reversing sign to -586 S/cm below the E_F . Similarly, the ANC reaches 0.34 A/mK at the E_F but increases to -2.61 A/mK below it.

4.2. Future Scope

These results highlight a pronounced sensitivity of both AHC and ANC to minor shifts in chemical potential, attributed to modifications in the Berry curvature distribution. Such behaviour underscores the critical role of electronic structure tunability in governing these transport coefficients. Therefore, our analysis identifies Co_2YSb as a new magnetic WSM candidate with the large AHE and ANE , making it a promising candidate for thermoelectric applications.

References

- [1] N. P. Armitage, E. J. Mele, and A. Vishwanath, ‘Weyl and Dirac semimetals in three-dimensional solids’, *Rev Mod Phys*, vol. 90, no. 1, p. 015001, Jan. 2018, doi: 10.1103/RevModPhys.90.015001.
- [2] B. Yan and C. Felser, ‘Topological Materials: Weyl Semimetals’, *Annu Rev Condens Matter Phys*, vol. 8, no. 1, pp. 337–354, Mar. 2017, doi: 10.1146/annurev-conmatphys-031016-025458.
- [3] A. A. Burkov, ‘Topological semimetals’, *Nat Mater*, pp. 1145–1148, 2016.
- [4] J. Cano, B. Bradlyn, and M. G. Vergniory, ‘Multifold nodal points in magnetic materials’, *APL Mater*, vol. 7, no. 10, Oct. 2019, doi: 10.1063/1.5124314.
- [5] Q. Xu, Z. Song, S. Nie, H. Weng, Z. Fang, and X. Dai, ‘Two-dimensional oxide topological insulator with iron-pnictide superconductor LiFeAs structure’, *Phys Rev B*, vol. 92, no. 20, p. 205310, Nov. 2015, doi: 10.1103/PhysRevB.92.205310.
- [6] W. Wu *et al.*, ‘Nodal surface semimetals: Theory and material realization’, *Phys Rev B*, vol. 97, no. 11, p. 115125, Mar. 2018, doi: 10.1103/PhysRevB.97.115125.
- [7] Z. Wang *et al.*, ‘Dirac semimetal and topological phase transitions in A₂Bi (A=nA, K, Rb)’, *Phys Rev B*, vol. 85, no. 19, p. 195320, May 2012, doi: 10.1103/PhysRevB.85.195320.
- [8] Z. K. Liu *et al.*, ‘Discovery of a Three-Dimensional Topological Dirac Semimetal, Na₃Bi’, *Science (1979)*, vol. 343, no. 6173, pp. 864–867, Feb. 2014, doi: 10.1126/science.1245085.
- [9] B. Q. Lv, T. Qian, and H. Ding, ‘Experimental perspective on three-dimensional topological semimetals’, *Rev Mod Phys*, vol. 93, no. 2, p. 025002, Apr. 2021, doi: 10.1103/RevModPhys.93.025002.
- [10] X. Wan, A. M. Turner, A. Vishwanath, and S. Y. Savrasov, ‘Topological semimetal and Fermi-arc surface states in the electronic structure of pyrochlore iridates’, *Phys Rev B*, vol. 83, no. 20, p. 205101, May 2011, doi: 10.1103/PhysRevB.83.205101.
- [11] Leon. Balents, ‘Weyl electrons kiss.’, *Physics*, vol. 4, p. 36, 2011.
- [12] G. Xu, H. Weng, Z. Wang, X. Dai, and Z. Fang, ‘Chern Semimetal and the Quantized Anomalous Hall Effect in HgCr_2Se_4 ’, *Phys Rev Lett*, vol. 107, no. 18, p. 186806, Oct. 2011, doi: 10.1103/PhysRevLett.107.186806.


- [13] O. Vafek and A. Vishwanath, ‘Dirac Fermions in Solids: From High- T_c Cuprates and Graphene to Topological Insulators and Weyl Semimetals’, *Annu Rev Condens Matter Phys*, vol. 5, no. 1, pp. 83–112, Mar. 2014, doi: 10.1146/annurev-conmatphys-031113-133841.
- [14] N. Nagaosa, J. Sinova, S. Onoda, A. H. MacDonald, and N. P. Ong, ‘Anomalous Hall effect’, *Rev Mod Phys*, vol. 82, no. 2, pp. 1539–1592, May 2010, doi: 10.1103/RevModPhys.82.1539.
- [15] L. Šmejkal, A. H. MacDonald, J. Sinova, S. Nakatsuji, and T. Jungwirth, ‘Anomalous Hall antiferromagnets’, *Nat Rev Mater*, vol. 7, no. 6, pp. 482–496, Mar. 2022, doi: 10.1038/s41578-022-00430-3.
- [16] D. Xiao, Y. Yao, Z. Fang, and Q. Niu, ‘Berry-Phase Effect in Anomalous Thermoelectric Transport’, *Phys Rev Lett*, vol. 97, no. 2, p. 026603, Jul. 2006, doi: 10.1103/PhysRevLett.97.026603.
- [17] W. Shi *et al.*, ‘Prediction of a magnetic Weyl semimetal without spin-orbit coupling and strong anomalous Hall effect in the Heusler compensated ferrimagnet Ti_2NiAl ’, *Phys Rev B*, vol. 97, no. 6, p. 060406, Feb. 2018, doi: 10.1103/PhysRevB.97.060406.
- [18] G. K. Shukla, U. Modanwal, and S. Singh, ‘Nodal-line symmetry breaking induced colossal anomalous Hall and Nernst effects in Cu_2CoSn Heusler compound’, *Appl Phys Lett*, vol. 123, no. 5, Jul. 2023, doi: 10.1063/5.0155940.
- [19] B. M. Ludbrook, B. J. Ruck, and S. Granville, ‘Perpendicular magnetic anisotropy in Co_2MnGa and its anomalous Hall effect’, *Appl Phys Lett*, vol. 110, no. 6, Feb. 2017, doi: 10.1063/1.4976078.
- [20] S. N. Guin *et al.*, ‘Anomalous Nernst effect beyond the magnetization scaling relation in the ferromagnetic Heusler compound Co_2MnGa ’, *NPG Asia Mater*, vol. 11, no. 1, p. 16, Dec. 2019, doi: 10.1038/s41427-019-0116-z.
- [21] H. Reichlova *et al.*, ‘Large anomalous Nernst effect in thin films of the Weyl semimetal Co_2MnGa ’, *Appl Phys Lett*, vol. 113, no. 21, Nov. 2018, doi: 10.1063/1.5048690.
- [22] T. Graf, C. Felser, and S. S. P. Parkin, ‘Simple rules for the understanding of Heusler compounds’, *Progress in Solid State Chemistry*, vol. 39, no. 1, pp. 1–50, May 2011, doi: 10.1016/j.progsolidstchem.2011.02.001.
- [23] T. Kono *et al.*, ‘Visualizing Half-Metallic Bulk Band Structure with Multiple Weyl Cones of the Heusler Ferromagnet’, *Phys Rev Lett*, vol. 125, no. 21, p. 216403, Nov. 2020, doi: 10.1103/PhysRevLett.125.216403.

- [24] R. Paudel and J. Zhu, ‘Investigation of half-metallicity and magnetism of bulk and (111)-surfaces of Fe₂MnP full Heusler alloy’, *Vacuum*, vol. 164, pp. 336–342, Jun. 2019, doi: 10.1016/j.vacuum.2019.03.049.
- [25] M. S. Alam *et al.*, ‘Sign change of anomalous Hall effect and anomalous Nernst effect in the Weyl semimetal CeAlSi’, *Phys Rev B*, vol. 107, no. 8, p. 085102, Feb. 2023, doi: 10.1103/PhysRevB.107.085102.
- [26] A. A. Burkov, ‘Anomalous Hall Effect in Weyl Metals’, *Phys Rev Lett*, vol. 113, no. 18, p. 187202, Oct. 2014, doi: 10.1103/PhysRevLett.113.187202.
- [27] L. Leiva *et al.*, ‘Efficient room-temperature magnetization direction detection by means of the enhanced anomalous Nernst effect in a Weyl ferromagnet’, *Phys Rev Mater*, vol. 6, no. 6, p. 064201, Jun. 2022, doi: 10.1103/PhysRevMaterials.6.064201.
- [28] K. S. Takahashi *et al.*, ‘Anomalous Hall effect derived from multiple Weyl nodes in high-mobility EuTiO₃ films’, *Sci Adv*, vol. 4, no. 7, Jul. 2018, doi: 10.1126/sciadv.aar7880.
- [29] H. Reichlova *et al.*, ‘Large anomalous Nernst effect in thin films of the Weyl semimetal Co₂MnGa’, *Appl Phys Lett*, vol. 113, no. 21, Nov. 2018, doi: 10.1063/1.5048690.
- [30] P. Li *et al.*, ‘Giant room temperature anomalous Hall effect and tunable topology in a ferromagnetic topological semimetal Co₂MnAl’, *Nat Commun*, vol. 11, no. 1, p. 3476, Jul. 2020, doi: 10.1038/s41467-020-17174-9.
- [31] S. Roy, R. Singha, A. Ghosh, A. Pariari, and P. Mandal, ‘Anomalous Hall effect in the half-metallic Heusler compound Co₂’, *Phys Rev B*, vol. 102, no. 8, p. 085147, Aug. 2020, doi: 10.1103/PhysRevB.102.085147.
- [32] R. P. Dulal, B. R. Dahal, A. Forbes, N. Bhattarai, I. L. Pegg, and J. Philip, ‘Weak localization and small anomalous Hall conductivity in ferromagnetic Weyl semimetal Co₂TiGe’, *Sci Rep*, vol. 9, no. 1, p. 3342, Mar. 2019, doi: 10.1038/s41598-019-39037-0.
- [33] O. Amrich *et al.*, ‘Half-Metallic Ferrimagnetic Characteristics of Co₂YZ (Z = P, As, Sb, and Bi) New Full-Heusler Alloys: a DFT Study’, *J Supercond Nov Magn*, vol. 31, no. 1, pp. 241–250, Jan. 2018, doi: 10.1007/s10948-017-4206-2.
- [34] G. Kresse and J. Furthmüller, ‘Efficient iterative schemes for *ab initio* total-energy calculations using a plane-wave basis set’, *Phys Rev B*, vol. 54, no. 16, pp. 11169–11186, Oct. 1996, doi: 10.1103/PhysRevB.54.11169.
- [35] G. Kresse and D. Joubert, ‘From ultrasoft pseudopotentials to the projector augmented-wave method’, *Phys Rev B*, vol. 59, no. 3, pp. 1758–1775, Jan. 1999, doi: 10.1103/PhysRevB.59.1758.

- [36] X. Wang, J. R. Yates, I. Souza, and D. Vanderbilt, ‘*Ab initio* calculation of the anomalous Hall conductivity by Wannier interpolation’, *Phys Rev B*, vol. 74, no. 19, p. 195118, Nov. 2006, doi: 10.1103/PhysRevB.74.195118.
- [37] J. P. Perdew, K. Burke, and M. Ernzerhof, ‘Generalized Gradient Approximation Made Simple’, *Phys Rev Lett*, vol. 77, no. 18, pp. 3865–3868, Oct. 1996, doi: 10.1103/PhysRevLett.77.3865.
- [38] S. S. Tsirkin, ‘High performance Wannier interpolation of Berry curvature and related quantities with WannierBerri code’, *NPJ Comput Mater*, vol. 7, no. 1, p. 33, Feb. 2021, doi: 10.1038/s41524-021-00498-5.
- [39] D. Xiao, M.-C. Chang, and Q. Niu, ‘Berry phase effects on electronic properties’, *Rev Mod Phys*, vol. 82, no. 3, pp. 1959–2007, Jul. 2010, doi: 10.1103/RevModPhys.82.1959.
- [40] K. Tang *et al.*, ‘Unconventional anomalous Hall effect and large anomalous Nernst effect in antiferromagnet SmMnBi₂’, *Commun Mater*, vol. 5, no. 1, p. 89, May 2024, doi: 10.1038/s43246-024-00525-0.
- [41] N. Nagaosa, J. Sinova, S. Onoda, A. H. MacDonald, and N. P. Ong, ‘Anomalous Hall effect’, *Rev Mod Phys*, vol. 82, no. 2, pp. 1539–1592, May 2010, doi: 10.1103/RevModPhys.82.1539.
- [42] L. Pauling, ‘The Nature of the Interatomic Forces in Metals’, *Physical Review*, vol. 54, no. 11, pp. 899–904, Dec. 1938, doi: 10.1103/PhysRev.54.899.
- [43] J. C. Slater, ‘The Ferromagnetism of Nickel. II. Temperature Effects’, *Physical Review*, vol. 49, no. 12, pp. 931–937, Jun. 1936, doi: 10.1103/PhysRev.49.931.
- [44] X. Zhang, B. Fu, L. Jin, X. Dai, G. Liu, and Y. Yao, ‘Topological Nodal Line Electrides: Realization of an Ideal Nodal Line State Nearly Immune from Spin–Orbit Coupling’, *The Journal of Physical Chemistry C*, vol. 123, no. 42, pp. 25871–25876, Oct. 2019, doi: 10.1021/acs.jpcc.9b08446.

APPENDIX

PLAGIARISM REPORT

Page 2 of 25 - Integrity OverviewSubmission ID trn:oid=27535:99622771





6% Overall Similarity

The combined total of all matches, including overlapping sources, for each database.




Filtered from the Report

- Bibliography
- Small Matches (less than 10 words)

Match Groups

-  **21 Not Cited or Quoted 6%**
Matches with neither in-text citation nor quotation marks
-  **0 Missing Quotations 0%**
Matches that are still very similar to source material
-  **1 Missing Citation 0%**
Matches that have quotation marks, but no in-text citation
-  **0 Cited and Quoted 0%**
Matches with in-text citation present, but no quotation marks

Top Sources

- 2%  Internet sources
- 5%  Publications
- 2%  Submitted works (Student Papers)

Integrity Flags

0 Integrity Flags for Review

No suspicious text manipulations found.

Our system's algorithms look deeply at a document for any inconsistencies that would set it apart from a normal submission. If we notice something strange, we flag it for you to review.

A Flag is not necessarily an indicator of a problem. However, we'd recommend you focus your attention there for further review.

Match Groups

- **21 Not Cited or Quoted 6%**
Matches with neither in-text citation nor quotation marks
- **0 Missing Quotations 0%**
Matches that are still very similar to source material
- **1 Missing Citation 0%**
Matches that have quotation marks, but no in-text citation
- **0 Cited and Quoted 0%**
Matches with in-text citation present, but no quotation marks

Top Sources

- 2% Internet sources
- 5% Publications
- 2% Submitted works (Student Papers)

Top Sources

The sources with the highest number of matches within the submission. Overlapping sources will not be displayed.

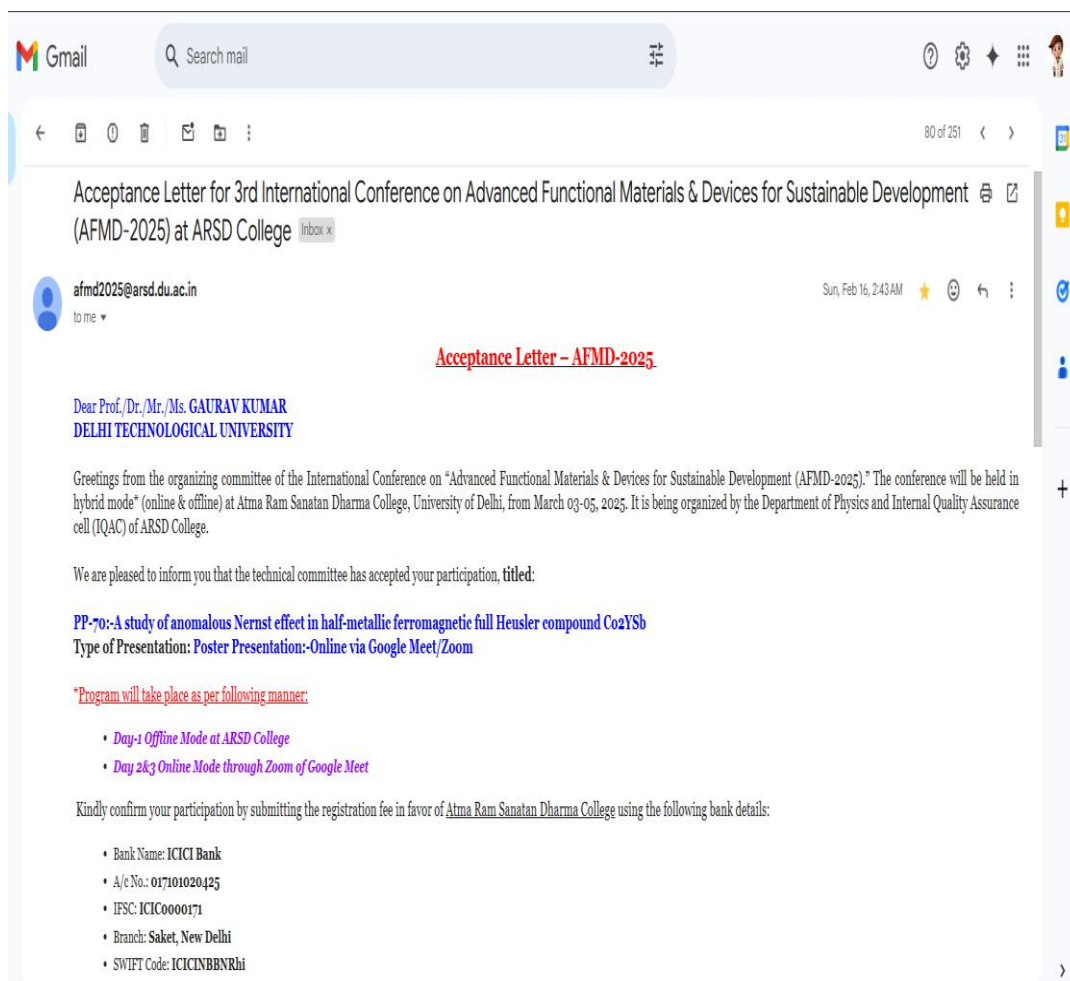
1	Internet	
	www.nature.com	<1%
2	Publication	
	Satya N. Guin, Kaustuv Manna, Jonathan Noky, Sarah J. Watzman et al. "Anomalo...	<1%
3	Publication	
	An-Qi Wang, Xing-Guo Ye, Da-Peng Yu, Zhi-Min Liao. "Topological Semimetal Nan...	<1%
4	Internet	
	repository.chuka.ac.ke	<1%
5	Publication	
	Asif Ullah, Thanh-Huong Thi Nguyen, Sanghoon Kim. "Observation of anomalous ...	<1%
6	Publication	
	A. Birsan. "Electronic structure and magnetism of new scandium-based full Heusl...	<1%
7	Publication	
	Chenguang Fu, Yan Sun, Claudia Felser. "Topological thermoelectrics", APL Materi...	<1%
8	Publication	
	Hai-Ming Huang, Zhen-Yi Jiang, Yong-Jin Hu, Wei Li, Shi-Jun Luo. "Effect of coulom...	<1%
9	Publication	
	Song-Bo Zhang, Jianhui Zhou. "Quantum oscillations in acoustic phonons in Weyl ...	<1%
10	Internet	
	docplayer.es	<1%

11	Publication	Teemu Ojanen. "Helical Fermi arcs and surface states in time-reversal invariant ..."	<1%
12	Submitted works	University of Minnesota System on 2025-05-10	<1%
13	Submitted works	Visvesvaraya National Institute of Technology on 2024-11-02	<1%
14	Publication	Ben Xu. "First-principles study on half-metallic properties of CuHg ₂ Ti-type alloys ..."	<1%
15	Publication	Congmin Wang. "Carbon Dioxide Capture by Superbase-Derived Protic Ionic Liqui..."	<1%
16	Publication	Liu, N., "Theoretical studies on the electronic structure and magnetic properties ..."	<1%
17	Publication	Yao Zhang, Yuefeng Yin, Guy Dubuis, Tane Butler, Nikhil V. Medhekar, Simon Gra...	<1%
18	Internet	docshare.tips	<1%
19	Internet	ia803104.us.archive.org	<1%

CERTIFICATE OF PARTICIPATION

 	<p>ATMA RAM SANATAN DHARMA COLLEGE UNIVERSITY OF DELHI</p> <p>Accredited Grade 'A++' By NAAC All India 5th Rank in NIRF (Ministry of Education)</p> <p><i>3rd International Conference on</i> Advanced Functional Materials and Devices (AFMD-2025) <i>for Sustainable Development</i></p> <p>Under the aegis of IQAC and supported by Department of Biotechnology (Govt)</p> <p><i>Certificate of Participation</i></p> <p>This is to certify that Prof./Dr./Mr./Ms. GAURAV KUMAR DELHI TECHNOLOGICAL UNIVERSITY</p> <p>has participated in the 3rd International Conference on "Advanced Functional Materials & Devices for Sustainable Development" (AFMD-2025) organised by Department of Physics under the aegis of IQAC ARSD College, University of Delhi, India during March 03-05, 2025 in hybrid mode.</p> <p>He/She has presented Poster entitled: PP-70:-A study of anomalous Nernst effect in half-metallic ferromagnetic full Heusler compound Co₂YSb</p> <table><tr><td> Dr. Shankar Subramanian Convener, AFMD-2025</td><td> Dr. Anjali Sharma Convener, AFMD-2025</td><td> Prof. Vinita Tuli Coordinator, IQAC</td><td> Prof. Gyantosh Kumar Jha Principal/Patron AFMD-2025</td></tr></table>	 Dr. Shankar Subramanian Convener, AFMD-2025	 Dr. Anjali Sharma Convener, AFMD-2025	 Prof. Vinita Tuli Coordinator, IQAC	 Prof. Gyantosh Kumar Jha Principal/Patron AFMD-2025	 
 Dr. Shankar Subramanian Convener, AFMD-2025	 Dr. Anjali Sharma Convener, AFMD-2025	 Prof. Vinita Tuli Coordinator, IQAC	 Prof. Gyantosh Kumar Jha Principal/Patron AFMD-2025			
Certificate No: ARSD/AFMD25/PP/073						

PROOF OF REGISTRATION



ABOUT THE CONFERENCE



3rd International Conference on Advanced Functional Materials and Devices for sustainable development (AFMD-2025)

Department of Physics and Internal Quality Assurance Cell (IQAC) of Atma Ram Sanatan Dharma College, University of Delhi



[HOME](#) [ABOUT](#) [COMMITTEES](#) [IMPORTANT DATES](#) [REGISTRATION DETAILS](#) [SPEAKERS](#) [PROCEEDINGS](#) [PROGRAM](#) [CONTACT](#) [DOWNLOADS](#)

About the College

Atma Ram Sanatan Dharma College, a prestigious institution under the University of Delhi, stands out with its remarkable achievements, including an All India NIRF Rank of 5 and NAAC A++ accreditation (3.77/4). Committed to nurturing academic excellence, the college fosters quality human resources and cultivates innovative ideas that benefit students. Since its establishment, ARSD College has been dedicated to character building and idealism, deeply rooted in Sanatani values. The college upholds inclusivity and equitability as its core principles, prioritizing the promotion of women's education and ensuring a supportive, barrier-free, and non-discriminatory environment for all. Additionally, ARSD College boasts a highly qualified faculty, excellent infrastructure, and a vibrant academic culture that encourages research, creativity, and extracurricular activities. The institution offers a wide range of undergraduate programs across various disciplines, catering to diverse academic interests. Its focus on skill development, career-oriented programs, and industry partnerships prepares students for global opportunities. Moreover, ARSD College actively engages in community service, sustainability initiatives, and cultural events, making it a hub of holistic education and personal growth.

About the Conference

After the successful completion of AFMD-2023, we are delighted to invite you to participate in the 3rd International Conference on Advanced Functional Materials and Devices for sustainable development (AFMD-2025), which will be held online from March 3 to 5, 2025. This conference follows the highly acclaimed events organized in March 2021 and March 2023. The primary objective of AFMD-2025 is to provide a global platform for researchers, academicians, scientists, and research students to exchange ideas, discuss breakthroughs, and share their latest achievements and innovations in the field of advanced functional materials and their applications in devices.

An abstract book will be published for the conference, and selected papers will undergo a rigorous review process conducted by the International Review Committee of AFMD-2025. Peer-reviewed and approved papers will be published in a proceedings book by Springer as part of their prestigious Scopus- and Web of Science-indexed series.

6/9/25, 6:41 AM

Gmail - Fwd: Acceptance Letter of Manuscript #AFMD-25-03073



Gaurav Kumar <gk743886@gmail.com>

Fwd: Acceptance Letter of Manuscript #AFMD-25-03073

1 message

Dr. Mukhtiyar Singh <mukhtiyarsingh@dtu.ac.in>

Mon, Jun 9, 2025 at 12:12 AM

To: Gaurav Kumar <gk743886@gmail.com>, kulwinder kumar <kk90344@gmail.com>

----- Forwarded message -----

From: **ARSD College** <afmd2025@arsd.du.ac.in>

Date: Sun, Jun 8, 2025 at 11:54 PM

Subject: Acceptance Letter of Manuscript #AFMD-25-03073

To: <mukhtiyarsingh@dtu.ac.in>

Paper ID: AFMD-25-03073

Paper Title: A theoretical study of Anomalous Nernst Conductivity with a Weyl-Semimetal Phase in Co₂YSb Heusler alloy

Status: Accepted

Dear Dr. Mukhtiyar Singh

We are delighted to inform you that your manuscript has been accepted for publication in its current form as a Springer Book Chapter (Scopus Indexed). Your manuscript will now proceed to the copy-editing and production stages.

Thank you for submitting your valuable work to the 3rd International Conference on Advanced Functional Materials and Devices for Sustainable Development (AFMD-2025). We look forward to your continued participation in future conferences at ARSD College.

Kind regards,

Editorial Team
AFMD-2025

--

Publications

Abstract book will be published.

All selected papers for AFMD 2025 will undergo the stringent review process by the International Review Committee of the AFMD 2025. The peer reviewed and selected papers of AFMD 2025 will be published by Springer with three different publishing houses.

1. Journal of Electronic Materials (Springer Nature Link) : Scopus Indexed (JEM Impact Factor: 2.2)

Note: Manuscripts will be evaluated according to the same high standards as would be applied to any article published in the journal. Authors are encouraged to read carefully and comply with the Instructions for Authors on the JEM website. All submitted papers will go through a plagiarism check to evaluate overlap with previously published work.

Manuscripts submitted after the deadline may not be considered for the publication.

2. Selected Proceedings Book Volume (Springer Nature, Singapore): Scopus Indexed

Selected papers for AFMD 2025 will undergo the stringent review process by the International Review Committee of the AFMD 2025. The peer reviewed and selected papers of AFMD 2025 will be published by Springer as a proceedings book volume. Springer will conduct quality checks on the accepted papers and only papers that pass these checks will be published. Springer Nature does not charge any money for publication of Non-Open Access content. Abstracts/extended abstracts and short papers (less than 4 pages) are not considered for publication.

3. Selected Proceedings Book Volume (Springer Nature, Switzerland with Capital Publishing): Scopus Indexed

Selected papers for AFMD 2025 will undergo the stringent review process by the International Review Committee of the AFMD 2025. The peer reviewed and selected papers of AFMD 2025 will be published by Springer as a proceedings book volume. Springer will conduct quality checks on the accepted papers and only papers that pass these checks will be published. Springer Nature does not charge any money for publication of Non-Open Access content. Abstracts/extended abstracts and short papers (less than 4 pages) are not considered for publication.

Detailed Guidelines will be share soon.

Click here to check our previous proceedings and publications:

1. [Recent Advances in Functional Materials and Devices: Select Proceedings of AFMD 2023 | SpringerLink](#)
2. [Advanced Functional Materials for Sustainable Environments | SpringerLink](#)